



1 Impacts of a large extra-tropical cyclonic system in 2 Southern Brazilian Continental Shelf using the COAWST 3 model

4 Luis Felipe F. Mendonça^{1,6,7}, Antônio F. H. Fetter-Filho², Mauro M. Andrade³, Fabricio S. C. Oliveira⁴,
5 Douglas S. Lindemann^{5,8}, Rose Ane P. Freitas⁵, Carlos. A. D. Lentini^{1,6,7}.

6
7 ¹ Federal University of Bahia – UFBA, Salvador, Brazil.

8 ² Federal University of Santa Catarina - UFSC, Florianópolis, Brazil.

9 ³ University of Itajaí - UNIVALI – Itajaí, Brazil.

10 ⁴ Federal University of Rio Grande - FURG, Rio Grande, Brazil.

11 ⁵ Federal University of Pelotas – UFPEL, Pelotas, Brazil.

12 ⁶ Tropical Oceanography Group – GOAT.

13 ⁷ Postgraduate Program in Geochemistry: Petroleum and Environment (POSPETRO) – UFBA, Salvador, Brazil

14 ⁸ Postgraduate Program in Meteorology – UFPEL, Pelotas, Brazil.

15 *Corresponding author:* Luis Felipe Mendonça (luis.mendonca@ufba.br)

16 **Abstract.** The Southern Brazilian Continental Shelf (SBCS) is an area with great ecological and economic
17 importance to Brazil. In this region can be observed the recurrent passage of frontal systems and
18 extratropical cyclones, which are more frequent during the winter months of the southern hemisphere. These
19 systems act on the ocean surface layers as direct driving forces, which may change the thermohaline
20 structure of the water column and induce sea level perturbations. This study used the coupled ocean-
21 atmosphere regional model (COAWST) to evaluate the effect of the passage of a frontal system associated
22 with an extra-tropical cyclone. The ocean and atmosphere models (ROMS and WRF) was configured with
23 two nested grids, in order to solve the dynamic processes, at different scales, that comprise the energy
24 transfer from the atmospheric system to the ocean. The simulation was based on a study case, occurred in
25 September 2016, on the southwestern brazilian continental shelf. The model outputs were
26 analyzed/compared to remote sensing data and 5 tide gauges from the Agricultural Research and Rural
27 Extension (EPAGRI) in Santa Catarina state, Brazil. This comparison showed a correlation higher than
28 78% between sea level rise data and the model results, with average difference of less than 25cm. The use
29 of low-pass Lanczos-Cosine filter made it possible to identify the meteorological component in the ocean
30 model outputs. Our simulation also presents the sea level anomalies, associated with the crossing of the
31 atmospheric frontal system, progressing to northward along the continental shelf at 480km.day⁻¹, probably
32 associated with the presence of a coastal-trapped wave.

33 1. Introduction

34 The Southern Brazilian Continental Shelf (SBCS) is located between the latitudes of 25°S and 33,74°S, it
35 is characterized by the frequent passage, formation, or intensification of frontal systems predominantly
36 from Chile, Argentina, and Uruguay (Gan & Rao 1991, Hoskins & Hodges 2005, Reboita *et al.*, 2010;
37 Krüger *et al.*, 2012, Escobar *et al.*, 2016 and Gramscianinov *et al.*, 2019). Several studies have shown that
38 the Southwest Atlantic Ocean has favorable atmospheric and oceanic conditions for cyclogenesis. These
39 conditions contribute to an intense exchange of sensible and latent heat between the two systems. These
40 phenomena have been the subject of several studies using observed data, reanalysis, global and regional



41 models (Bitencourt *et al.*, 2011; Gozzo e Rocha, 2013; Rosa *et al.*, 2013; Gozzo *et al.*, 2014; Rocha *et al.*,
42 2018; Reboita *et al.*, 2019; Reboita *et al.*, 2020).

43 Cyclogenesis are recurring features on the Southwest Atlantic Ocean at mid-latitudes and can be observed
44 throughout the entire year, being more frequent between May and September (Escobar *et al.*, 2016). The
45 passage of frontal systems may be accompanied by cyclones and anticyclones, which change the pressure,
46 wind, and other atmospheric variables. Using data from ERA-Interim, Machado *et al.* (2020) indicated that
47 storms on the southern Brazilian coast are accompanied by strong winds causing intense disturbance on the
48 sea surface. These synoptic systems have a highly destructive potential, with strong winds hitting the
49 coastline, lasting from hours up to days. One of the most well documented phenomenon of this kind was
50 the Catarina Cyclone. This system generated winds in excess of $150\text{km}\cdot\text{h}^{-1}$ and inflicted considerable
51 damage to the infrastructure of several cities along the southeastern coast of Brazil, during March 2004.
52 The strong winds associated with the passage of these systems have a direct impact on the sea surface and
53 generate instability in the mixing layer, changing the circulation and transport in the coast (Stech &
54 Lorenzetti, 1992; Castro & Lee, 1995; Innocentini & Caetano Neto, 1996; Rocha *et al.* 2004).

55 The winds on the SBCS are a first order forcing to the local oceanic circulation, in which the wind stress
56 and Ekman transport are responsible for water movements at different time scales (Moller, *et al.* 2008). The
57 local wind accounts for 90% of sea level changes along the coast and one of this sea level rise is associated
58 with the meteorological tide (technically known as non-astronomical component). In the time scales of
59 interest in this work, the atmosphere can induce sea level variations through two mechanical effects: (i)
60 pressure (inverse barometer effect) of the atmosphere over the ocean (Wunsch e Stammer, 1997) and (ii)
61 drag (tangential tension) caused by the wind tension on the sea surface (Dean & Dalrymple, 1991).

62 Large variations in the coastal sea level are associated with these meteorological events that induce the
63 generation of coastal-trapped waves (e.g., Kelvin waves) and intensify the coastal currents system. Frandry
64 *et al.* (1984) analyzed sea level data and found evidence that the observed storm surges were associated
65 with the propagation of coastal-trapped waves, although their theoretical analysis was for a flat-bottomed
66 ocean, hence allowing only the propagation of Kelvin waves. Tang & Grimshaw (1995) analyzed coastal
67 trapped waves generated by intense atmospheric systems, such as extratropic cyclones, and their results
68 show that wave fields are dominated by lower-mode shelf waves. They observed that the large-scale
69 response is predominantly due to shelf waves, while Kelvin waves are confined to transient wave fronts.

70 There are not many studies investigating the formation of coastal-trapped waves in the SBCS, Saraceno *et al.*
71 *et al.* (2005) showed intra-seasonal peaks in the frequencies of SST and chlorophyll, suggesting coastal
72 trapped waves as a possible mechanism leading to the observed variability.

73 Hoskins & Rodges (2005) analyzed systems that lasted longer than 2 days and moved more than 1000km
74 and concluded that the storm tracks in Southern Hemisphere (SH) are important for latitudinal transports
75 and the dynamic of the Southern Ocean. This hypothesis was derived from many studies of the SH storm
76 tracks that showed the genesis of eastward-moving cyclonic systems at latitudes higher than 25°S ,



77 traversing the southwestern flanks of the subtropical anticyclones and changing the atmospheric layer over
78 the SBCS. In the years 2008 and 2010, the occurrence of these events caused severe damage to the facilities
79 and operations of the Port of Itajaí and Navegantes due to floods (Casagrande, *et al.*, 2017). The recurrence
80 of such phenomena requires the development of monitoring programs and tools for projecting and
81 monitoring the impact that extreme events can have on coastal communities.

82 According to Chelton *et al.* (2004) data from remote sensing of SST and wind on the surface revealed that
83 the ocean-atmosphere coupling mechanisms are fundamentally different in the small and mesoscale analysis
84 compared to the basin scales processes. Maloney & Chelton (2006), examined the ability of climate models
85 to simulate the positive correlation between SST and the magnitude of the wind stress at the ocean surface.
86 However, due to the lower resolution of the global models it is not possible to simulate the exchanges and
87 variations of SST and SSH at the scale of the processes necessary for a study on the continental shelf
88 (Taguchi *et al.*, 2012). Gronholz *et al.* (2017) showed that these differences can cause notable changes to
89 ecosystem modeling, since the coupled ocean-atmosphere model can better determine coastal circulation,
90 the development of biological processes after a storm or simulate sedimentary transport over a continental
91 shelf. In addition, the atmospheric circulation components of the coupled model are able to simulate local
92 circulation patterns and exchange processes much more effectively (Cocke & Larow, 2000).

93 Based on this, we use a coupled ocean-atmosphere model to simulate the occurrence of a strong
94 extratropical cyclone formed over the southwest Atlantic Ocean, near the mouth of La Plata River, from 12
95 to 15 September 2016. This cyclone induced a large accumulation of water on the coast, initially in the La
96 Plata River next to the Uruguayan coast, transferring its energy across the SBCS like a coastal-trapped
97 wave. In this event, the cities of Florianópolis and Itajaí, in the State of Santa Catarina, had several areas of
98 flooding, as shown in Figure 1. The years 2015 and 2016 were characterized by the occurrence of the
99 positive phase of the El Niño South Oscillation (ENSO) phenomenon, with strong intensity. According to
100 Ambrizzi *et al.* (2004) there is no evidence of an increase in cyclogenesis in ENSO years, but there is an
101 increase in the region where the cyclone occurs between 30°-60°S, which comprises our study area. The
102 southern states of Brazilian coast are prone to the frequent passage of frontal systems and the formation of
103 extratropical cyclones. These systems often cause flooding and socio-economic losses to the coastal areas
104 as described by Machado *et al.* (2011); Evans & Braun (2012) and Guimarães *et al.*, (2014).



105
106 Figure 1 - Flood in the city of Florianópolis on 15 September 2016. Source: Executive Secretariat of
107 Communication and Civil Police Air Service.



108 The present study uses a regional coupled ocean-atmosphere numerical simulation, aiming to reproduce the
109 coastal ocean circulation during the meteorological event of September 2016. For this simulation, we used
110 an ocean-atmosphere coupled model with a nested grid that comprises the coast of Santa Catarina State
111 (Fig. 2), in Brazil. This region was chosen due to existence of tide-gauge data from the Agricultural
112 Research and Rural Extension (EPAGRI), kindly made available to use in the validation of the model. The
113 simulation results were used to investigate the impacts of energy transfer from the atmosphere to the SBCS
114 waters, as well as the sea level variability produced along the coastal region, during the passage of the
115 frontal system.

116 2. Materials and Methods

117 2.1. Characterization of the study area

118 The circulation over the South Atlantic Ocean is controlled by a high-pressure center associated with the
119 Hadley cell, called the South Atlantic Subtropical High (SASH) (Sun, *et al.*, 2017). This system varies
120 seasonally and directly influences the climate in the southern and southeastern regions of Brazil, showing
121 a connection between SST anomalies and precipitation on the Southwest Atlantic Ocean (SWAO) (Diaz *et al.*,
122 1998). The seasonal profile of winds on the SWAO is strongly associated with the SASH latitudinal
123 variation. According to Hoskins & Hodge (2005), the SWAO is one of the main regions influenced by
124 extra-tropical cyclones, anticyclones, and droughts in the SH, especially during winter. The Southwest
125 Atlantic Ocean are constantly affected by the passage of cold-air masses and extra-tropical cyclones. The
126 ocean-atmosphere coupling in mid-latitudes under a strong wind regime induces turbulent mixing and
127 changes the conditions of the mass transport of marine currents over the entire SBCS (Camargo *et al.*,
128 2013).

129 The SBCS is characterized by a regular morphology, that presents a soft slope and establishes a smooth
130 passage to the upper continental slope (Zenbruski *et al.*, 1972). The ocean circulation on the SBCS is
131 characterized by the presence of the Brazil Current, western boundary current of the subtropical gyre of the
132 South Atlantic Ocean (Matano *et al.*, 2014). The Brazilian Current (BC) is formed at approximately 16°S
133 and flows to the south/southwest (Wienders *et al.*, 2000). In the opposite direction to the BC, the Malvinas
134 Current (MC) is a faster current that flows to north/northeast parallel to the Argentine shelf break and carries
135 between 40Sv and 70Sv (Fetter & Matano, 2008; Matano *et al.*, 2010). The collision of these two currents
136 occurs at approximately 38°S, the so-called Brazil-Malvinas Confluence (Fetter & Matano, 2008; Matano
137 *et al.*, 2010). The shelf circulation consists of a flow of cold waters from the south – transporting the
138 subantarctic Shelf Water (SASW) – and a flow of hot waters from the north – carrying the Subtropical Shelf
139 Water (STSW) – that are constantly fed by the BC (Piola *et al.*, 2000; Palma *et al.*, 2008). Shelf subantarctic
140 waters have thermohaline characteristics that are different from those transported by the MC and their
141 velocities are substantially smaller (Piola *et al.*, 2010).

142 In the SBCS the internal circulation is regulated by the local wind, while the BC plays a major role in the
143 mid and outer shelf regions (Palma & Matano, 2009; Matano *et al.*, 2010). During the winter, winds from
144 the south quadrant induce mixing between the SASW and the La Plata River Plume (PRP), forming a



145 strongly seasonal marine current, called the Brazilian Coastal Current (BCC), over the continental shelf
146 region north of the La Plata River mouth (Souza & Robinson, 2004). This current is forced by the local
147 wind and by the river discharge from the La Plata River (average runoff of $24,000\text{m}^3\cdot\text{s}^{-1}$) and Patos-Mirim
148 (average runoff of $2,000\text{m}^3\cdot\text{s}^{-1}$) water systems, creating a unique thermohaline profile on the Uruguayan
149 continental shelf and on the northern SBCS (Matano *et al.*, 2014).

150 The astronomical tides on the SBCS have mean amplitudes of 0.4m and 1.2m for the neap and spring tide
151 periods, respectively. The astronomical tide is mixed with a semi-diurnal predominance and presents height
152 inequalities, the small tidal amplitude is associated with the proximity to an amphidromic point (for M2) in
153 the South Atlantic Ocean. Due to meteorological forcing, sea level may raise up to 1m above the predicted
154 astronomical tide (Truccolo *et al.*, 2004). The southern Brazilian region is constantly affected by the
155 crossing, formation and intensification of atmospheric fronts. These transient meteorological systems move
156 over this region, changing the fields of temperature, pressure, wind, waves and are responsible for the
157 transfer of momentum for the formation of meteorological tides (Wallace & Hobbs, 1977). Meteorological
158 tides are very frequent and have different amplitudes on the southern Brazilian coast (Andrade *et al.*, 2018).
159 Explosive cyclogenesis near the south coast of Brazil are the main causes of storm surges on the coast.
160 These phenomena in the region occur throughout the year, but more frequently during winter months. The
161 main mechanism responsible for transferring energy from the atmosphere to the ocean is through the friction
162 of the winds on the sea surface, which associated with the force of Coriolis and the oceanic mesoscale
163 gyration, cause the accumulation of water in the coast (Pugh, 1987). Storm surges amplify the occurrence
164 of erosive processes and floods over the coastal region (Parise *et al.*, 2009). Natural disasters and extreme
165 events are already a reality in Brazil and the diagnosis of their occurrences are an important tool to guide
166 and improve policies of coastal management.

167 **2.2. Numerical Simulation**

168 The southern Brazilian coast is characterized by synoptic winds, dominated by mesoscale processes
169 associated mainly with the passage of frontal systems. Despite of the acceptable performance of some global
170 models to simulate these conditions, the oceanic characteristics of SBCS require a regional model capable
171 of representing the intensification of winds by processes of exchange between the ocean and the atmosphere
172 (Perlin *et al.*, 2011). Gronholz *et al.* (2017) showed that the interactions in the mixing layer, during and
173 after the crossing of a synoptic system, in an uncoupled simulation, with lower spatial resolution, do not
174 represent satisfactorily the shelf environments. In turn, a coupled simulation is able to mix the entire water
175 column with higher resolution of data. Therefore, in this study a coupled ocean-atmosphere model system
176 was used, in order to better represent the complex shelf circulation dynamics associated with the passage
177 of frontal systems.

178 The model setup and the validation methodology are similar to those used by Mendonça *et al.* (2017), since
179 the authors used the same parameterization of the ocean and atmosphere models, essential to guarantee the
180 quality of the simulation. The current understanding of coastal processes is largely based on numerical
181 models, which mathematically reproduce the dynamic conditions of a region of interest. The present study



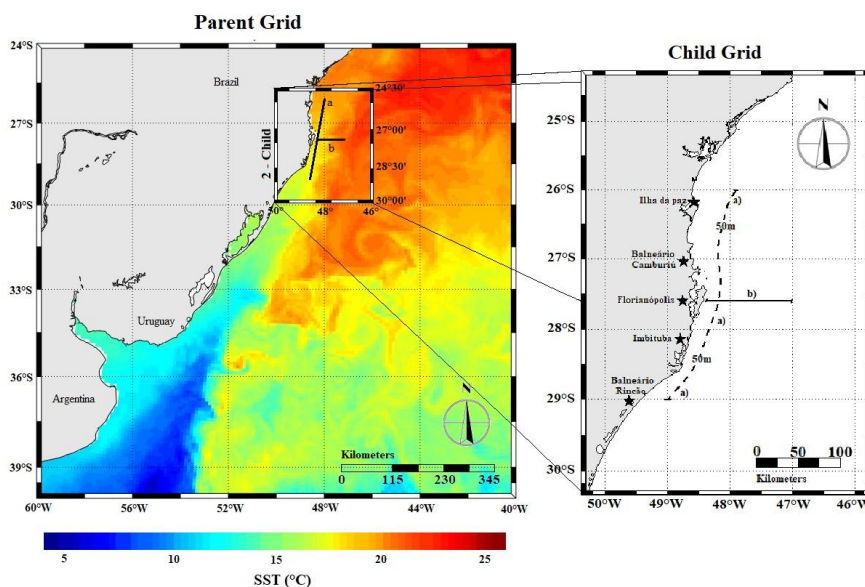
182 used the coupled ocean-atmosphere modules from the *Coupled Ocean Atmosphere Wave Sediment*
183 *Transport* (COAWST) model system (Warner *et al.*, 2008). The ocean module is composed by the *Regional*
184 *Ocean Modeling System* (ROMS) (Haidvogel *et al.*, 2000; Shchepetkin & McWilliams, 2005, 2009) and
185 the atmospheric module corresponds to the *Weather Research and Forecast* (WRF Model Version 4.0.3).
186 WRF is a non-hydrostatic, fully compressible atmospheric model that has a range of parameterizations and
187 terrain-following mass-based, hybrid sigma-pressure vertical coordinate based on dry hydrostatic pressure,
188 with vertical grid stretching permitted (Powers *et al.*, 2017). The wave and sediment transport modules
189 were not used in these simulations because this paper is focused only on the oceanic component of
190 COAWST. Even though surface gravity waves are important for determining the momentum transfer from
191 the atmosphere to the ocean, this work does not include that process, for a series of reasons: absence of long
192 surface gravity waves data in the region to validate the model results; the poorly known topography at the
193 model resolution to properly resolve surface gravity waves; the introduction of one more layer of
194 parametrization with scarce data to corroborate the results. Adding too many degrees of freedom to a system
195 sometimes leads to apparently correct results, with the wrong physics. ROMS constitutes a three-
196 dimensional regional ocean model of free surface that uses the finite-difference method, solving the
197 Reynolds-Medium and Navier-Stokes equations with the Boussinesq and the hydrostatic approximations.
198 The model uses an Arakawa-C grid with a mask for coast delimitation and sigma vertical coordinates
199 (Shchepetkin & McWilliams, 2005).

200 The ROMS oceanic model was configured with two nested grids: a mid-resolution parent grid and a coastal,
201 high-resolution, child grid (Fig. 2). The parent grid was intended to solve the main meso and large-scale
202 circulation, as well as the set-up/set-down mechanisms associated with the wind on the SBCS and adjacent
203 ocean. On the other hand, the child grid was chosen to better resolve the coastal processes of the SBCS
204 region. The ocean parent grid comprised the coastal region between 20–40°S and 40–60°W, with a
205 horizontal resolution of 1/9°. The child grid embraced the region in 25–29.3°S by 46.3–50°W, with a
206 horizontal resolution of 1/27°, both grids had 32 sigma vertical levels. It should be pointed out that the child
207 grid was not centered on the parent grid, the reason being that: the location of the south open boundary of
208 the parent grid was chosen in order to include the La Plata River and its inflow, which are important for
209 determining the circulation of this part of the South American Continental Shelf; the north open boundary
210 of the parent grid was chosen to be far enough from the north open boundary of the child grid, in order to
211 avoid contamination of the child grid solution by inevitable reflections that occur at any open boundary.

212 The ROMS initial conditions are from Copernicus - GLOBAL Ocean Sea Physical Analysis and Forecasting
213 Products (GLOBAL_ANALYSIS_FORECAST_PHYS_001_024 - Global Ocean 1/4° Physics Analysis
214 and Forecast Updated Daily), available in <https://resources.marine.copernicus.eu>. At the three open
215 boundaries (N-S-E, Fig. 2) the solution was nudged to data from the same Copernicus Product which were
216 imposed every hour at a horizontal resolution of 1/4°. The bathymetry used was from the ETOPO1 - Global
217 Relief Model (Amante & Eakins, 2009) provided by the *National Centers for Environmental Information*
218 (NCEI). The tidal harmonic components (M2, S2, N2, K2, Q1, O1, P1, K1, M4, MS4, and MN4) from the
219 tidal model *OSU TOPEX/Poseidon Global Inverse Solution* (TPXO) (Egbert & Erofeeva, 2010), version



220 7.2, were applied at the open boundaries. This work shows the statistically stable state attained by this
221 model and its capability of representing the oceanographic characteristics of the SBCS.



222
223 **Figure 2** – Study area and the two nested grids: a) parent and child grids and b) child grid. Colored contours
224 represent the mean SST modeled for the period between 11 and 19 September 2016. The child grid has 2
225 transects used to identify the coastal-trapped wave: a) meridional transects along the 50m isobath on the
226 continental shelf between 26–29°S; b) zonal transect at 27°40'S.

227 The WRF regional atmospheric model was configured with a similar grid to the ocean model, having a
228 12km horizontal resolution and 38 isobaric vertical levels. The chosen Micro Physics Option is *WRF*
229 *Single-moment 3-class and 5-class Schemes* (Hong *et al.*, 2004), Planetary Boundary Layer Scheme is
230 Yonsei University Scheme (YSU) (Hong, *et al.*, 2006), cumulus parameterization was Kain–Fritsch
231 Scheme (2004), shortwave and longwave parametrization is Dudhia (1989) and RRTM (Mlawer, *et al.*,
232 1997), respectively, Land Surface option is NOAH (Niu, *et al.*, 2011). According to Kleczek, *et al.* (2014)
233 the adequate time for a spin-up is estimated based on the initialization conditions, that is, it can be affected
234 by the domain range and by the disturbances of the local limits. Based on previous sensitivity studies, the
235 official WRF website recommends a 12h turnaround time as the initial state. According to the developers,
236 this is the most suitable condition in many case studies without further verification. In this study, the model
237 spin-up lasted 24h and two more days of simulation before the occurrence of the extratropical cyclone
238 object of this study. The model was integrated for 198h with a time step of 72s and output interval of 3h –
239 according to the empirical calculation described by Skamarock *et al.* (2008).

240 To perform the coupled simulation, it is necessary to adjust the frequency with which the models exchange
241 information with each other via Bulk-type parameterizations. For this simulation, the interval of information
242 exchange between the models was 300s, so that the parameterizations and adjustments were extracted



243 individually from each model during the simulation. In order to stabilize the ocean model kinetic and
244 potential energies, one spin-up of 5 years was run as from 10 September 2011, with initial and boundary
245 conditions of the Mercator Global Analysis Forecast and forced by CFSv2. This process kept running until
246 the solution reached a quasi-equilibrium state, as suggested by Kantha & Clayson (2000). The final spin-
247 up conditions were used as the initial condition in oceanic model of COAWST to run the simulations from
248 10 to 18 September 2016, with hourly outputs subsequently validated according to the following
249 methodology.

250 2.3. Data validation

251 To assess the hindcast accuracy of the model, two data validation steps were performed. The first one
252 consisted of comparing temperature and sea surface elevation from the model output with remote sensing
253 data. The SST data used in this comparison was from the *Optimum Interpolation Sea Surface Temperature*
254 (OISST), version 2 (Reynolds *et al.*, 2007), which corresponds to a series of daily products of global
255 analysis from the *National Oceanic and Atmospheric Administration* (NOAA). The AVHRR-OI product
256 uses an Optimum Interpolation (OI) analysis system on the infrared data measured by the *Advanced Very*
257 *High-Resolution Radiometer* (AVHRR) sensor (Pathfinder versions 5.0 and 5.1) combining observations
258 from satellites, ships and buoys on a regular global grid. This product was available daily at a horizontal
259 resolution of $1/4^\circ$ (Casey *et al.* 2010), spatially gridded through data interpolation and extrapolation,
260 resulting in a complete, smoothed SST field. Data from remote and *in situ* platforms were statistically
261 adjusted to fill non-existent values on satellite product, usually caused by the frequent cloud coverage in
262 the region, especially in winter.

263 The use of interpolated data and multi-channel sensors is considered fundamental to study this region. The
264 altimetric data were from the *Near-Real Time and Delayed Time* products from *AVISO* at $1/4^\circ$ resolution,
265 available in <https://www.aviso.altimetry.fr>. These data consist of series of daily products of global analysis
266 from the *Center National d'Études Spatiales* (CNES) and is calculated with an ideal computing time
267 window centered at 6 weeks, before and after the acquisition date. The data acquisition was performed
268 through a sequence of ten daily images that corresponded to the period from 10 to 20 September 2016. The
269 data were stored without pre-processing and resized to meet the same number of grid points from the ocean
270 model in order to subsequently perform a pixel-by-pixel comparative analysis. Finally, the Bias and Root
271 Mean Square Error (RMSE) statistics were performed with later plotting of the observed values.

272 The second validation step consisted of comparing the model surface elevation (zeta) to tide gauges from
273 the pilotage of the Rio Grande Port, located in Rio Grande (32.13°S – 52.10°W), pilotage of the Tramandaí
274 (RS), located in Tramandaí (29.98°S – 50.13°W), Agricultural Research and Rural Extension of Santa
275 Catarina (EPAGRI), located in the cities of Balneário Rincão (28.83°S – 49.23°W), Imbituba (28.13°S –
276 48.40°W), Florianópolis (27.59°S – 48.54°W), Balneário Camburiú (27.00°S – 48.63°W) and São Francisco
277 (26.20°S – 48.50°W). The grid point closest to the coordinates of the tide station was chosen and the analysis
278 of the astronomical tide and subtidal components was performed for the period from September 10 to 18,
279 2016. The raw data were processed using a Lanczos-Cosine low-pass filter (Thompson, 1983), which

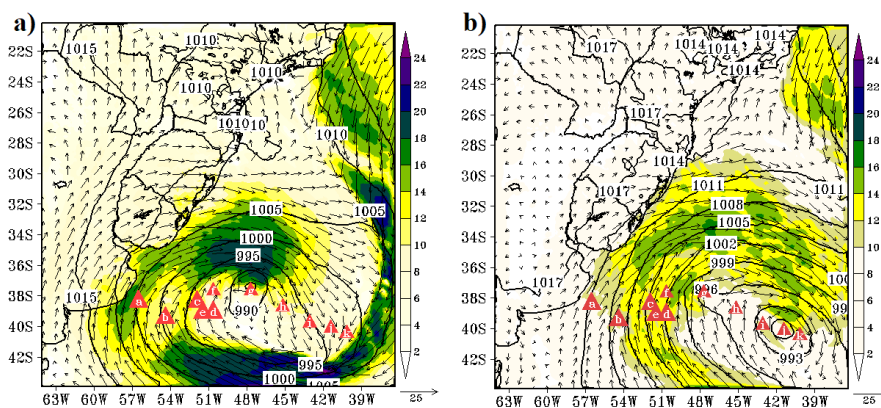


280 removes 95% of oscillations higher than 40h^{-1} . This process is responsible for separating the high-frequency
281 (tidal) from low-frequency (subtidal) components that are associated with an active meteorological system.
282 Based on the distinction between tidal and subtidal data, the comparison and the statistical analysis of Bias
283 and RMSE were performed during the period of interest.

284 3. Results and Discussion

285 3.1 – Atmospheric Analysis

286 The analysis of the atmospheric conditions was carried out using synoptic charts from the Center for
287 Weather Forecast and Climate Studies (CPTEC-INPE), from 10 to 18 September 2016, available in
288 <http://tempo.cptec.inpe.br/cartas.php?tipo=Superficie>. Fig. 3 shows a transient synoptic system present in
289 the Southwest Atlantic Ocean (SWAO), significantly changing the mean atmospheric circulation of this
290 region. The Figure 3 describe the track of the atmospheric system since the formation of the extratropical
291 cyclone over the ocean, until the displacement offshore on 15/09/2016. A low-pressure center was observed
292 in 12/09/2016, this system moved zonally (close to 32°S) from Argentina towards Brazil. Afterwards the
293 low-pressure center moved southeastwards (00h on 13/9/2016), at this point as an extratropical cyclone on
294 the east coast of Argentina, as indicated by the letter “a”. During 13/09/2016, the cyclone intensified to the
295 east of the Argentinean city of Mar del Plata, the sea level pressure values ranged from 996hPa at 00h to
296 975hPa at 00h on 14/9/2016, with a pressure drop of 21hPa in 24h, which was classified as a kind of
297 explosive cyclogenesis (Dal Piva *et al.*, 2011; Reale *et al.*, 2019; Schossler *et al.*, 2020).



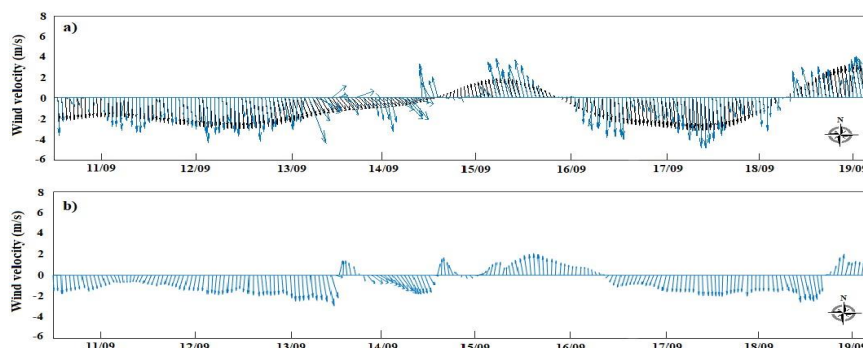
298
299 Figure 3 - Representation of the extratropical cyclone that occurred near the coast of southern Brazil,
300 Uruguay and Argentina, during 12-15 September 2016: a) 12h on 14/9/2016; b) 06h on 15/9/2016. Red
301 triangles represent the center of the cyclone every 6h, "a" represents 00h on 13/09/2016, and "k" represents
302 12h on 15/09/2016. Vectors indicate wind speed and direction ($\text{m}\cdot\text{s}^{-1}$), areas filled with magnitude and black
303 lines indicate pressure at sea level (hPa).

304 Strong winds from the southwest quadrant reached the coastlines of Argentina and Uruguay during
305 13/09/2016 (letters "a" to "d"), reaching up to $24\text{m}\cdot\text{s}^{-1}$ at 18h. The intense southwest winds on 13/9/2016



306 piled the waters up at the mouth of La Plata River, against the Uruguayan coast. The southern part of Rio
307 Grande do Sul State coast (Brazil) felt the influence of the extratropical cyclone, with winds from the west
308 quadrant $10\text{--}12\text{m.s}^{-1}$. The cold front associated with the extratropical cyclone caused precipitation in this
309 region according to meteorological stations of the National Institute of Meteorology (INMET), with
310 accumulations between $30\text{--}40\text{mm}$. During 14/09/2016, the extratropical cyclone moved offshore and the
311 winds on the coast of Rio Grande do Sul began to intensify, reaching values of 14m.s^{-1} at 12h, when the
312 cyclone was at the “f” position (Figure 3a). At 18h on 14/9/2016, when the extratropical cyclone was at the
313 “g” position, the southern Santa Catarina coast was hit by winds influenced by the low-pressure system,
314 with speeds close to 10m.s^{-1} . More intense winds were observed at 06h on 15/09/2016, while the cyclone
315 was moving offshore (letter “j”), with an average wind speed between $10\text{--}14\text{m.s}^{-1}$ (Figure 3b), the system
316 lost strength during the day, reaching 10m.s^{-1} at 18h on 15/9/2016, at this point the cyclone was out of the
317 study region.

318 In the afternoon of 15/09/2016, the INMET meteorological station, located in the City of Florianópolis
319 (A806), in Santa Catarina State ($28.60^{\circ}\text{S}\text{--}48.81^{\circ}\text{W}$), recorded winds with speeds between $10\text{--}11\text{m.s}^{-1}$.
320 During the extratropical cyclone crossing, 12 to 15/09/2016, the correlations between the WRF output and
321 the meteorological station data were 0.57 and 0.97, for the wind speed next to the surface and sea level
322 pressure, respectively. Figure 4 presents the wind direction and intensity for the studied period, comparing
323 the data obtained through the outputs atmospheric model and the INMET automatic meteorological station
324 of Florianópolis (A806). The large variation in the wind direction of the meteorological station data,
325 required the filtering of high frequency data (Figure 4a – black arrow), so that we could better understand
326 the impact of the Ekman transport and storm surge. The greatest variations in sea level data and wind
327 intensity were analyzed in a synoptic scale for the study region. The cyclone west border remained active
328 in Santa Catarina coast until 16/09/2016, intensifying winds from the south-southwest (S-SW) quadrant on
329 the southern coast of Brazil. After 16/09/2016, the extra-tropical cyclone lost strength and moved
330 southeastward of the study area, maintaining its high pressure until 18/09/2016.



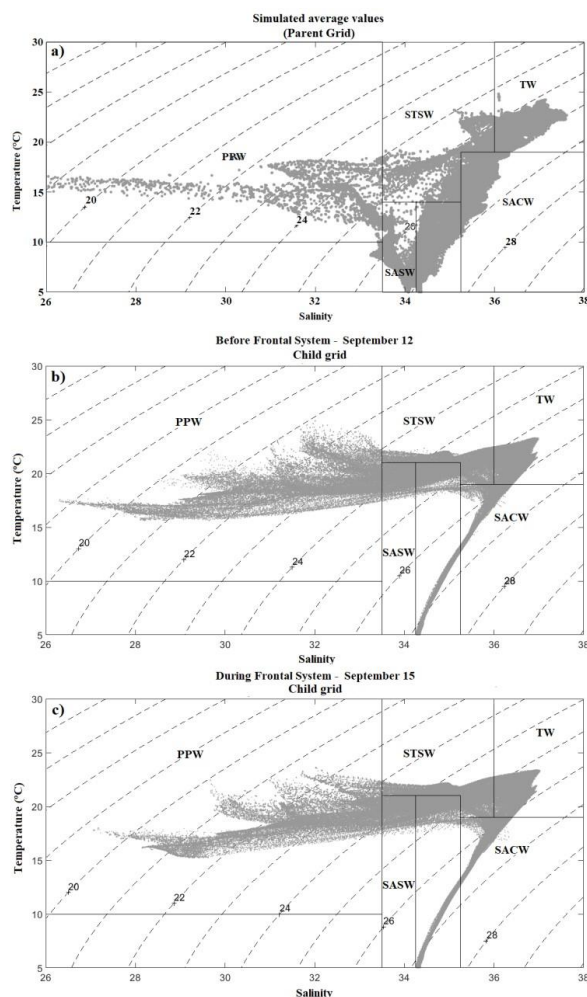
331
332 **Figure 4** – a) INMET meteorological station in the City of Florianópolis/São José (A806) - the blue arrows
333 indicate raw data wind speed (m.s^{-1}) and the black arrows are the filtered wind data, without the high
334 frequency of directional variations; b) output from the meteorological model (WRF) at the same position
335 of the INMET meteorological station.



336 3.2 Oceanic Analysis

337 Figure 5a shows the T/S scatter diagram, of the parent grid, with average model output values for the SBCS
338 region, calculated from 11 to 19 September 2016. Data were plotted with the thermohaline indices described
339 by Möller *et al.* (2008) to characterize the main water masses on the SBCS. According to this
340 characterization, it is possible to observe that the numerical model was able to represent the main water
341 masses in the study region: PRP, SASW, Subtropical Shelf Water (STSW), Tropical Water (TW), and South
342 Atlantic Central Water (SACW). It should be pointed out that, even during the spring, the presence of the
343 SASW in latitudes higher than 35°S indicates a slow retraction of the Brazilian Coastal Current (BCC, not
344 shown) as described by Souza & Robinson (2004), Piola *et al.* (2005, 2008), Möller *et al.* (2008), and
345 Matano *et al.* (2010). The T/S diagram data points that corresponded to the SASW and STSW were
346 concentrated at the edges of the characterization boxes, showing that the mixing occurs gradually over the
347 continental shelf as demonstrated by Möller *et al.* (2008) and Mendonça *et al.* (2017).

348 Figures 5b and 5c shows the T/S scatter diagram with the modeled data on the continental shelf of the State
349 of Santa Catarina (child grid) before and during the passage of the atmospheric system. According to
350 Pingree & Mardell (1981) in stratified shelf waters, the mixture caused by internal waves, due to the
351 barotropic tides, plays a role in cooling the shelf break and in releasing nutrients. In addition to the wind
352 induced resurgence, the increase in phytoplankton growth can occur under improved light conditions, where
353 nutrients and phytoplankton are released into surface waters along the shelf break region. During the
354 analyzed period, there was a large volume of Plata Plume Waters (PPW), which were transported during
355 the winter by the BCC (Souza & Robinson, 2004). Figure 5b shows the presence of the lighter La Plata
356 Plume Waters, with lower densities, especially at the surface. Figure 5c may be showing that more intense
357 winds increase the mixing layer and the surface salinity, through mixing with STSW. The statistical analysis
358 of the grid points showed that there was an increase of 8% in the total volume of STSW on continental shelf
359 of the child grid, compared to the period before the cyclone. The deepening of the mixing layer moves the
360 SACW towards the bottom towards the shelf break (Piola, 2008). This process shows that the increase in
361 turbulence in the shallow shelf waters can be an important mechanism for adding nutrients to the water
362 column, with direct impact on primary productivity as described by Alcaraz, *et al.* (2002) and Saldanha-
363 Corrêa & Giancesella (2004).

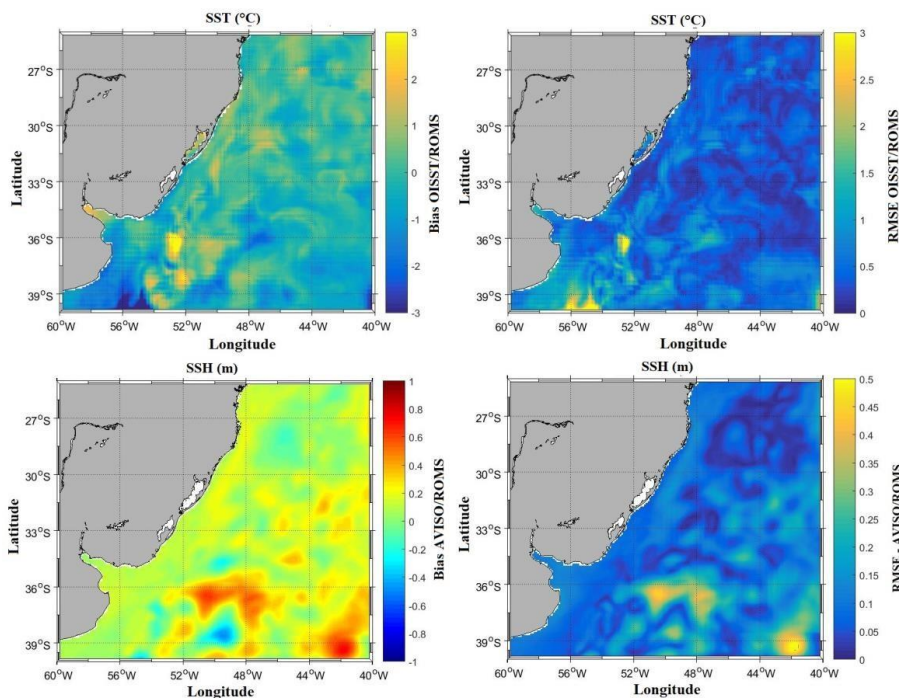


364
365 **Figure 5** – (a) T/S scatter diagram presenting the average model output data (gray dots). Shaded lines
366 represent sigma-T values (density). The names of the water masses and the thermohaline limits were
367 described by Möller *et al.* (2008). (b) Model output data of child grid before crossing the frontal system in
368 12/09/2016 and (c) after crossing the frontal system, 15/09/2016.

369 The differences between OISST and modeled data were relatively small, presenting a mean Bias that ranged
370 from -1.5 to 1.5°C (Figure 6). The differences remained constant both on the SBSC and in the open ocean,
371 showing greater values in the thermal gradient region of BMC. RMSE was between 0–1°C, which
372 corresponds to a good agreement between model and data over the entire time series. Mendonça *et al.*
373 (2017) obtained RMSE values higher than 2.5°C for the BMC region during 2012. The presence of eddies
374 and meanders in the BC core, described by Mascarenhas *et al.* (1971), follows the continental shelf contours
375 along the entire grid. High RMSEs near the BMC demonstrates the lack of skill of the model on reproducing
376 the mesoscale variability of the BMC, in agreement with Souza & Robinson (2004). The instabilities caused



377 by the thermal gradient between tropical (BC) and subantarctic (MC) waters on the surface generate distinct
378 mesoscale features such as meanders and eddies (Legeckis & Gordon, 1982; Lentini *et al.*, 2000).



379
380 **Figure 6** – BIAS and RMSE calculated from the SST and SSH from the model outputs and remote sensing.

381 The comparison between satellite and modeled SSH data showed mean differences between -0.2 and 0.2m
382 on the SBCS and offshore, which were close to those found by Hermes & Reason (2005). The typical high
383 frequency periodicity in tidal data may combine with the lower sampling frequency of the altimeter and
384 cause distortions or associated errors, which can lead to the presence of low-frequency artificial signals in
385 the sampled time series (Strub *et al.*, 2015). This concern with tidal errors is greater where tides are large
386 (Palma *et al.*, 2004, 2008), although it is possible to occur significant errors in conditions similar to the area
387 of this study. Due to the short period of this analysis, we do not have consistent data for a more detailed
388 analysis of the greatest differences in sea level variation of SBCS, however the largest bias were found in
389 the south of the grid near the BMC, associated with the presence of meanders and large-scale eddies (Olson
390 *et al.*, 1988).

391



392 **3.3 Tide-gauge Analysis**

393 The second validation step of the coupled model was to compare the surface elevation values from the
394 model, with the data from EPAGRI tide stations in cities of Balneário Rincão, Imbituba, Florianópolis,
395 Balneário Camburiú e São Francisco, during the period of formation and crossing of frontal system over
396 the studied period. Figure 7 shows the results of the low-frequency components of all datasets, which were
397 obtained by filtering the data with a 39h (the inertial period of the location) low-pass Lanczos filter. The
398 high-frequency oscillations were obtained by subtracting the subtidal frequencies from the raw series. In
399 this case, there is a correlation between coastal winds and sea level, with significant coherence at all
400 frequencies. By analyzing the low frequency components of Figure 7, in Florianópolis, we can identify that
401 there is a relationship between the variation of the level and the resultant of the wind presented in Figure
402 4b. We observed, in the Florianópolis region, the occurrence of a synchrony between the crossing of
403 southern coastal winds and the rise in sea level around the 15th of September. As expected, there is a ~6h
404 delay between the start of the wind action and the change in sea level.

405 The results showed a satisfactory agreement between the time series and the model, both at the tidal and
406 subtidal frequency range. The largest differences appeared at high frequencies, where the model intensified
407 the effects of the astronomical tides. However, the model was able to simulate with reasonable efficiency
408 the mean low-frequency oscillations (Pearson correlation = 0,78), which are mainly forced by the
409 alongshore wind. Low-frequency sea level records have been widely used to study continental shelf
410 dynamics and its relationship with the wind and atmospheric pressure. The majority of sea level variations
411 associated with low-frequency subtidal components are driven by wind stress and Ekman transport
412 (Truccolo *et al.*, 2004). These oscillations cause a cross-shelf barotropic gradient, which is geostrophically
413 balanced with the alongshore current (Thompson, 1981; Stech & Lorenzetti, 1992).



414

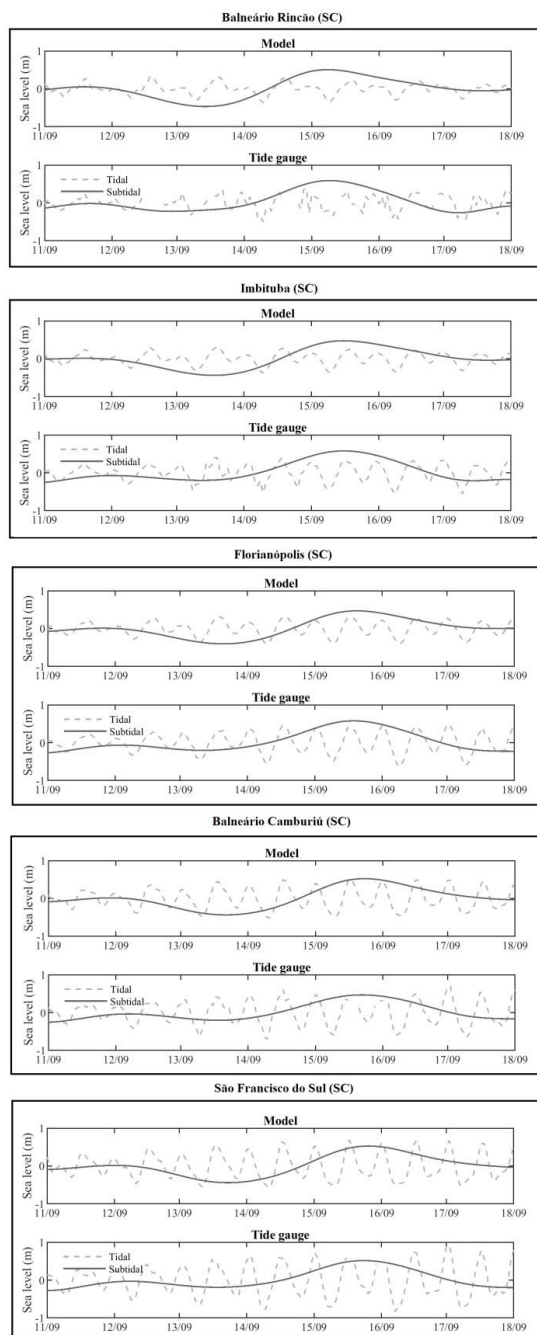


Figure 7 - Temporal variation of the tidal and subtidal components of sea level from the numerical model and from the tide gauges of EPAGRI in the cities of Balneário Rincão, Imbituba, Florianópolis, Balneário Camburiú e São Francisco.

3.4 Coastal Wave Occurrence

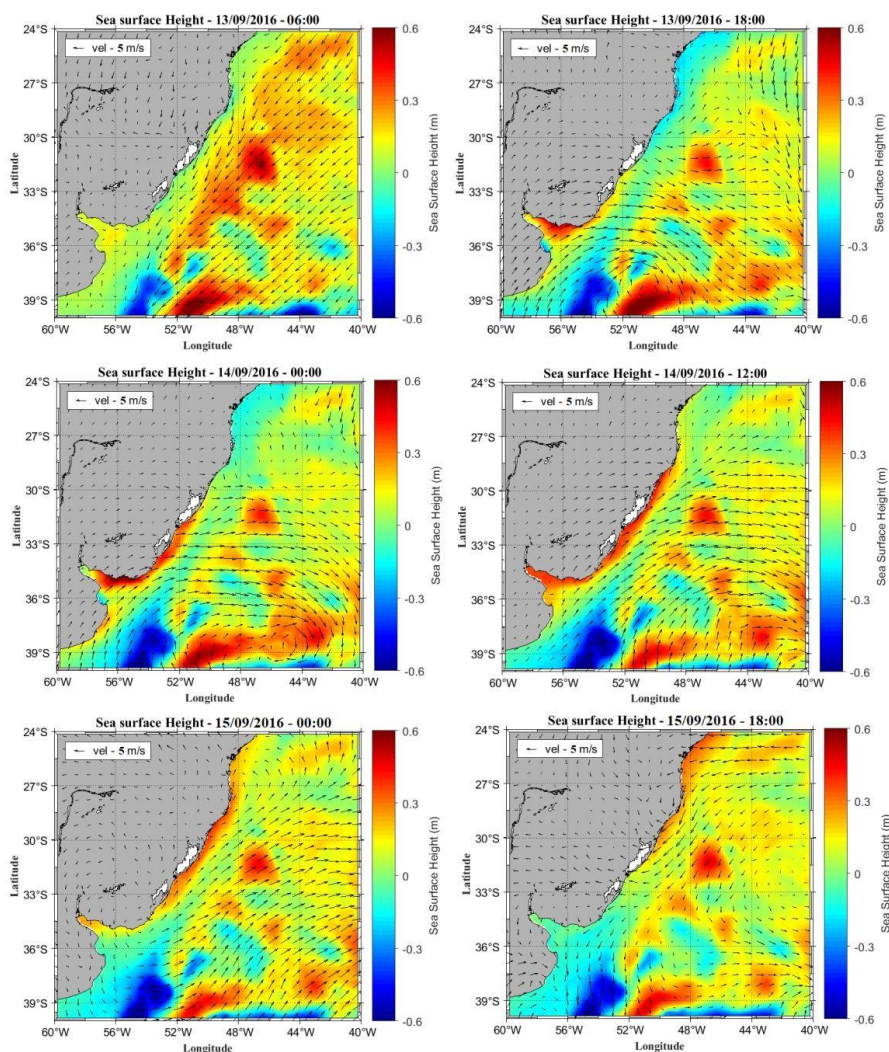
Tang & Grimshaw (1995) showed that transient atmospheric systems can induce the accumulation of coastal waters, which are formed through the geostrophic flow generated by coastal trapped waves. In our work, the analysis of the extratropical cyclone indicates that the atmospheric system generated a sea level variation by two mechanical effects: (i) atmospheric pressure on the ocean (normal tension) and (ii) drag caused by the wind tension on the sea surface (tangential stress). The process of sea level rise started in the La Plata estuary, after the fast formation of the low-pressure core of the extratropical cyclone, as shown in Figure 3. The atmospheric pressure drops, quickly, from 1008hPa (12/09/2016 – 12h) to 990hPa 24h later. According to Pontes & Gaspar (1999), the response of sea level to surface atmospheric pressure is commonly followed by an inverted

449 barometer phenomenon, with an estimated elevation of 1cm for each 1hPa, indicating an induced local
450 elevation of ~0.2m. Figure 8 shows that at 18h, on 13/09/2016, the elevation in La Plata River mouth was



451 approximately 0.5m, near the Uruguayan coast. Therefore, in addition to atmospheric pressure, the
452 horizontal movement of the south wind caused by the western boundary of the cyclone, disturbed the
453 equilibrium condition of the ocean. The stress transmitted into the fluid promoted a momentum transfer
454 from the atmosphere to the ocean (Dean & Dalrymple, 1991), overcoming the inertial period for the region
455 of ~20h, increasing the effect of wind set-up on the coast.

456 The physical mechanism that explains the force of the coastal-trapped waves over topography is
457 straightforward, wind stress along the coast causes transport within the Ekman layer. Then mass
458 conservation generates a compensating offshore flow in the lower layer. As this flow crosses the isobaths,
459 it leads to changes in the local relative vorticity, which is expressed in terms of velocity along the coast and,
460 in the presence of variability along the coast, it generates the propagation of the waves (Brink, 1991). In the
461 southern hemisphere, topographic Rossby waves propagate with the coast at its left, thus progressing to the
462 north along the western continental margin of South America. Gill & Clarke (1974), Schumann (1983), and
463 Batisti & Hickey (1984) argued that the alongshore component of the wind stress is the main creator and
464 enhancer of such trapped waves. Consequently, those waves share the same periods with the meteorological
465 systems that caused them. The winds formed by the gradient of the low-pressure centers created by the
466 cyclone are the main modulating mechanisms of positive variations in sea level (Calliari *et al.*, 1998). At
467 00h, on 14/09/2016, it was possible to observe the displacement of a surface elevation anomaly, originated
468 at the Uruguayan coast, towards north (Fig. 8). The analyses of the surface elevation anomalies shows that
469 the winds of the extra-tropical cyclone intensified the coastal trapped wave, which continued to propagate
470 towards the State of Santa Catarina even after the winds ceased (15/09/2016 -18h).



471
472 Figure 8 - Maps of the subtidal components of sea surface elevation and wind fields generated by the
473 numerical model, at specific dates, during the passage of the frontal system.

474 Melo *et al.* (2008) showed that extra-tropical cyclones formed far from the Brazilian coast can reach it and
475 induce significant changes in sea level and Parise (2009) identified an extra-tropical cyclone in the South
476 Atlantic Ocean that contributed over 70% of the energy of the wave spectrum along the coast of RS. In order
477 to show the propagation of the costal-trapped wave, the subtidal components from the EPAGRI tide gauges
478 (Figure 9a) and from the numerical model (Figure 9b) were plotted over time. As EPAGRI tide stations
479 cover only the Santa Catarina state, we can see in Figures 3 and 8, that the probable formation area of this
480 trapped wave over the River Plate, near the Uruguayan coast. Thus, were also plotted for numerical model,



481 in dashed lines, data on the coast of Montevideo (UY), Rio Grande (BR) and Paranaguá (BR) for analysis
482 of wave propagation before and after the passage through the State of Santa Catarina.

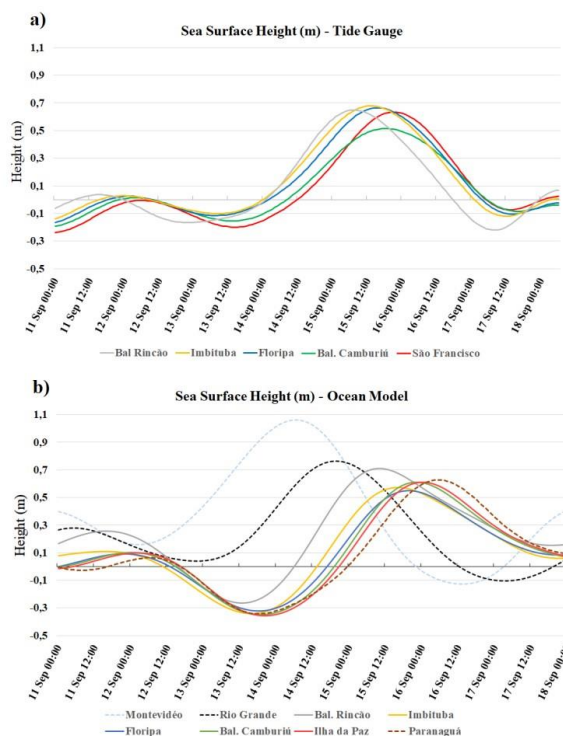
483 Figure 9 shows the SSH anomalies associated with the storm surge where it is possible to identify four peaks.
484 They present a time lag of a few hours and an advance towards the north, probably associated with a coastal
485 trapped wave. A cross-correlation analysis made it possible to identify the time lag of these elevations along
486 the coast. Through the average time of signal movement between analyzed points it is possible to estimate
487 the average speed of propagation in relation to the distance covered by the wave. Using the distance among
488 the sites and considering that the peak of maximum correlation indicates the wave time lag, it was possible
489 to estimate the average propagation speed of the trapped wave generated by the storm surge. Therefore,
490 since the cyclone formed near the La Plata river mouth, this site was considered as the region where the
491 winds originated or intensified the amplitude of the analyzed trapped wave. The numerical model generated
492 a coefficient of determination in the range of 78%, slope of the regression line close to the ideal value (1.00),
493 with a standard deviation of less than 10 cm. According to Brink (1991), the existing models tend to
494 underestimate the amplitude of observed fluctuations in the current along the coast and at sea level, usually
495 by around 10-50%. The wave propagation velocity analyzes showed higher velocity values ($\sim 10.6 \text{ m}\cdot\text{s}^{-1}$)
496 over the continental shelf of Uruguay and Rio Grande do Sul. Keeping more than $10 \text{ m}\cdot\text{s}^{-1}$ until Imbituba.
497 From Imbituba, until Paranaguá, the speed values decreased to $\sim 6 \text{ m}\cdot\text{s}^{-1}$ due, we believe, to the change in
498 the direction of the coastline, reduction of the slope and the widening of the continental shelf.

499 The integration was carried out over the eight locations represented in Figure 9. The speed of the phase
500 decreases over time with the reduction of winds from the extratropical cyclone. We can see that the sea level
501 rise in Montevideo (UY) starts around 12h on 12/09/2016, possibly forced by the effect of the inverted
502 barometer observed in the pressure fields of the WRF model. The advance of the low frequency coastal
503 wave is seen in Figure 8, in tide gauge and the model outputs, following the wind fields (S-SW) of the extra-
504 tropical cyclone and seems to be responsible for the formation and/or intensification of these waves on
505 SBCS. In the comparative analysis between the tide gauges data and numerical model we can observe similar
506 periods of maximum amplitudes. However, in the cases of Balneário Rincão and Balneário Camburiú, there
507 were overestimations of the model up to 0.1m above that observed by the tide gauge. We believe that these
508 differences may be associated with the position of the coastline or the collection of data in more external
509 areas in relation to the original position of the tide gauge. Based on the signal speed along the coast, we can
510 see that there are similarities in the energy distribution between each of the stations observed, through a
511 coherence and phase relationship along the continental shelf of Santa Catarina.

512 Figure 9 shows a good qualitative agreement between the data and the model, there are, however, some
513 important differences between model and observations. The data and the model show an evident propagation
514 of the SSH signal towards north, with the wave first reaching the southern cities of the study region. The
515 model, however, propagates the wave faster than it was observed from the tide gauges data, it is clear that
516 the model maximum elevation leads the tide gauge data by a few hours. This is probably due to the poor
517 topography of the region and possibly the limited model resolution. The tide gauge data also shows a fast



518 reduction of the wave amplitude after passing the city of Florianópolis and arriving at Balneário Camboriú
519 (less than 100km to the north).



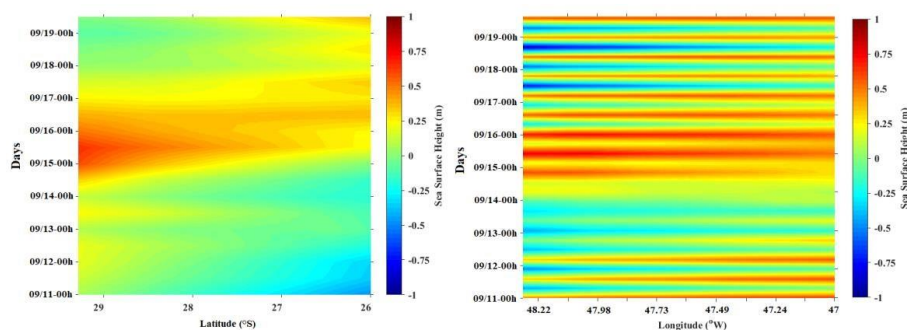
520
521 **Figure 9** – Temporal variation of SSH data: a) tide gauges in Balneário Rincão, Imbituba,
522 Florianópolis, Balneário Camboriú e São Francisco and b) numerical model in Montevidéo, Rio Grande,
523 Balneário Rincão, Imbituba, Florianópolis, Balneário Camboriú, Ilha da Paz e Paranaguá, SC. Maximum
524 amplitude of waves for the analyzed period.

525 Figure 10 shows the Hovmöller diagrams of sea surface elevation, during the period from 11 to 19 September
526 2016. Figure 10a was generated using data from an alongshore transect (Fig. 2) over the 50m isobath –
527 without the tidal component – in order to evaluate the evolution of the wave trapped to the continental shelf
528 of Santa Catarina. The wind started changing its direction from the north-northeast (N-NE) quadrant to the
529 S-SW one after 00h on 13/09/2016. The sea surface elevation followed the S-SW wind fields and at 00h on
530 14/09/2016 the consequent impact of the storm surge was observed in the coastal waters of Balneário
531 Rincão. The gradual advance of this elevation to the northeast with a coherent period suggests the formation
532 of a coastal-trapped wave, as noted by Houghton & Beer (1976), Brink (1991), Battisti & Hickey (1984),
533 Yao *et al.* (1984), Kitade & Matsuyama (2000) and Junker *et al.* (2019).

534 The retraction of the coastline, close to 27.5°S, induced this wave to move away from the coast, but without
535 a significant increase in depth. The widening of the continental shelf in this region increased the elevation



536 area offshore, without significantly reducing the wave amplitude. The subtidal component generated SSH
537 values above 0.5m as seen on the Hovmöller diagram along the entire Santa Catarina coast. That agreed
538 with the tidal data released by the EPAGRI company from region, which recorded a residual height close to
539 ~0.6m associated with coastal wave created by storm surge. Figure 10b shows the Hovmöller diagram of
540 free surface variation from a cross-shore profile near the coast of Florianópolis (28°S). The SSH values were
541 under a tidal regime. These data showed high-frequency oscillations and elevations of up to 1m during
542 maximum S-SW wind intensity. Despite the astronomical tide daily oscillations, the storm surge component
543 had a significant impact on sea level rise in this region. According to Truccolo *et al.* (2004), low-frequency
544 sea level oscillations play an important role along the coast of SC because the astronomical component is
545 microtidal. It is even possible to observe the augmentation of the neap tide during the period when the N-
546 NE winds are prevailing on the region.



547
548 **Figure 10** – Hovmöller diagrams of SSH temporal variation. (a) Diagram generated without the tidal
549 components from an alongshore transect, over the 50m isobath, on the coast of Santa Catarina state, between
550 the latitudes of 26 and 29°S. (b) Diagram generated from a cross-shore transect over the latitude of 28°S
551 with the tidal components.

552 According to Möller *et al.* (2008) and Piola *et al.* (2008), the local wind changes the current speeds and
553 transport along the SBCS. Costa & Möller (2011) and Andrade *et al.* (2016) used data from acoustic profilers
554 to show that the direction of currents on the SBCS oppositely change throughout the water column a few
555 hours after the change in wind direction. Dias *et al.* (2014) added that it is not only the offshore Ekman
556 transport that is responsible for the physical-chemical changes on the SBCS, but the coastline geometry is
557 also important. Studies such as Figueiredo Jr. (1980), Zavialov *et al.* (2002), Costa & Moller (2011), and
558 Andrade *et al.* (2016) have shown the impact that the passage of an intense atmospheric system can cause
559 on the local hydrodynamics, especially on shallow waters driven by winds that are associated with the frontal
560 system. Rodrigues *et al.* (2004) showed that cold fronts move on the SBCS from southeast to northeast with
561 a monthly frequency of 3-4 fronts/month, usually followed by mobile cyclones and anticyclones (Wallace
562 & Hobbs, 1977). Therefore, the changes caused by these atmospheric systems have a direct influence on the
563 coastal environment, altering the thermohaline structure and oxygenating the coastal waters. The increase



564 in the number of studies on the impact of the passage of frontal systems on the SBCS may, in the near future,
565 provide new answers to still unresolved questions regarding the southern Brazilian coastal system.

566 4. Conclusions

567 The present work presented the implementation of the coupled ocean-atmosphere model for studying a
568 specific process of ocean-atmosphere interactions on the continental shelf from the state of Santa Catarina,
569 during the passage of a frontal system associated with an extra-tropical cyclone in September 2016. The
570 solution used boundary components adjusted for the conditions from an earlier study (Mendonça *et al.*,
571 2017). The presented findings demonstrated regional circulation patterns strongly associated with the
572 meteorological conditions present in the southern Brazilian region. These processes change the physical and
573 chemical properties of sea water, changing the mixing layer and fertilizing the shelf waters.

574 The analyzed period consisted of the rapid formation of an extra-tropical cyclone on the parent grid,
575 intensifying the south-quadrant winds and the associated Ekman transport. The rapid drop in pressure levels
576 on the La Plata River has generated an increase in sea level, caused by the inverted barometer, that was
577 intensified by the winds from the south-southwest quadrant. The low-frequency components were found to
578 be the controlling mechanism of the model elevation output. The filtering of the model altimetric data
579 allowed the identification of the storm surge component (low frequency) with a short lag in relation to the
580 tide gauge data. This process was important to identify the advance of a coastal wave (Figure 8 and 9),
581 intensified by the winds from the frontal system responsible for flooding several cities along the coast of
582 Santa Catarina.

583 The analysis of maximum correlation between the peaks of sea level elevation – at the eight analyzed sites
584 was superior to 82%. Although the relationship between wind forcing, wave, and the resulting flux is not
585 linear, the correlation coefficient gives us a measure of the wave propagation behavior on the continental
586 shelf (Fewings, 2007). According to Brink (1991), a qualitative assessment delineated the conditions for the
587 development of large waves trapped to the coast and associated with tropical cyclones: when the storm
588 moves for several hours, its translation speed slowly increases, continuously matching the group velocity of
589 the waves under the storm. The strong correlation between winds and the current at the surface and on the
590 bottom shows a rapid response of the water to wind forcing. The results obtained with the application of the
591 COAWST model agreed with the estimates from other authors although the dynamic arguments of the
592 momentum equation were not considered due to the size limitations of this manuscript. Since the southern
593 region of Brazil is constantly affected by the passage of frontal systems, studies capable of interpreting the
594 changes in the SBCS dynamics have great importance for the ecological characterization and the prevention
595 of coastal impacts associated with sea level variations.

596



597 **Acknowledgments**

598 We thank CNPq and INCT-Mar COI for funding in the form of a postdoctoral fellowship. The main
599 author, as a faculty member, would like to thank the Pos-graduate Program in Geochemistry of Petroleum
600 and Environment (POSPETRO) at the Federal University of Bahia. Thank all the researchers and students
601 of the Laboratory of Dynamic Oceans of the Federal University of Santa Catarina. To thank the Agricultural
602 Research and Rural Extension Company of Santa Catarina, which provided free of charge the tide data and
603 Dr. Elírio Ernestino Toldo Junior (Federal University of Rio Grande do Sul) for the sea level data provided
604 together with Prof. Dr. Mauro Michelena Andrade (Univali). The output data of the numerical model used
605 in this study are available in web repository ([https://1drv.ms/u/s!AhHBbFlJz9g7BapIYB3ifwgFqqSA-
606 ?e=RqKgSh](https://1drv.ms/u/s!AhHBbFlJz9g7BapIYB3ifwgFqqSA-?e=RqKgSh)).

607

608 **References**

- 609 Alcaraz, M.; Marrasé, C.; Peters, F.; Arin, L.; Malits, A.: Effects of turbulence conditions on the balance
610 between production and respiration in marine planktonic communities. *Mar. Ecol. Progr. Ser.*, 242:63-71,
611 2002.
- 612 Amante, C. & Eakins, B. W.: ETOPO1 1 Arc-Minute Global Relief Model: Procedures, Data Sources and
613 Analysis. NOAA Technical Memorandum NESDIS NGDC-24. National Geophysical Data Center, NOAA.
614 doi:10.7289/V5C8276M, 2009.
- 615 Ambrizzi, T.; Souza, E. B.; Pulwarty, R S.: The Hadley and Walker regional circulations and associated
616 ENSO impacts on the South American Seasonal Rainfall. In: Henry F. Diaz; Raymond S. Bradley. (Org.).
617 The Hadley Circulation: Present, Past and Future. 1 ed. Netherlands: Kluwer Academic Publishers, v. 21,
618 p. 203-235, 2004.
- 619 Andrade, M. M.; Toldo E. Jr.; Nunes, J. C.: Variability of currents on the inner shelf of Tramandaí (RS)
620 during the summer of 2014. *Geoscience Research*, 43, 4, 289-298, 2016.
- 621 Andrade, M. M.; Toldo, E. E.; Nunes, J. C. R.: Tidal and subtidal oscillations in a shallow water system in
622 southern Brazil. *Brazilian Journal of Oceanography*, 66(3), 245-254, 2018.
- 623 Battisti, D. S. & Hickey, B. M.: Application of remote wind-forced coastal trapped wave theory to the
624 Oregon and Washington coasts. *Journal of Physical Oceanography*, 14, 5, 887-903, 1984.
- 625 Bitencourt, D. P.; Manoel, G.; Acevedo, O. C.; Fuentes, M. V.; Muza, M. N.; Rodrigues, M. L.; Leal
626 Quadro, M. F.: Relating winds along the Southern Brazilian coast to extratropical cyclones. *Meteorological
627 Applications*, 18(2), 223-229, 2011.
- 628 Brink, K. H.: Coastal-trapped waves and wind-driven currents over the continental shelf. *Annual Review
629 of Fluid Mechanics*, 23(1), 389-412, 1991.



- 630 Calliari, L. J.; Tozzi, H. A. M.; Klein, A. H. F.: Beach morphology and coastline erosion associated with
631 storm surge in Southern Brazil-Rio Grande to Chuí, RS. *Annals of the Brazilian Academy of Science*, 70,
632 2, 1988.
- 633 Camargo, R.; Todesco, E.; Pezzi, L. P.; Souza, R. B.: Modulation mechanisms of marine atmospheric
634 boundary layer at the Brazil-Malvinas Confluence region. *Journal of Geophysical Research - Atmospheres*,
635 118, 12, 6266–6280, 2013.
- 636 Casagrande, L.; Tomasella, J.; dos Santos Alvalá, R. C.: Early flood warning in the Itajaí-Açu River basin
637 using numerical weather forecasting and hydrological modeling. *Nat Hazards* 88, 741–757.
638 <https://doi.org/10.1007/s11069-017-2889-0>, 2017.
- 639 Casey, K. S.; Brandon, T. B.; Cornillon, P.; Evans, R.: The past, present, and future of the AVHRR
640 Pathfinder SST program. In *Oceanography from space*, Springer Netherlands, 273-287, 2010.
- 641 Castro, B & Lee, T.: Wind-forced sea level variability on the southeast Brazilian shelf. *Journal of*
642 *Geophysical Research*, 100, 16045–16056, 1995.
- 643 Costa, R. & Möller, O. O.: Study of the structure and variability of currents in the area of the inner shelf off
644 Rio Grande (RS, Brazil), southwest of the South Atlantic during spring-summer 2006-2007. *Journal of*
645 *Integrated Coastal Zone Management*, 11, 3, 273-281, 2011.
- 646 Cocke, S. & LAROW, T. E.: Seasonal predictions using a regional spectral model embedded within a
647 coupled ocean-atmosphere model. *Monthly Weather Review*, v. 128, n. 3, p. 689-708, 2000.
- 648 Dal Piva, E.; Gan, M. A.; de Lima Moscati, M. C.: The role of latent and sensible heat fluxes in an explosive
649 cyclogenesis over the South American East Coast. *Journal of the Meteorological Society of Japan. Ser.*
650 *II*, 89(6), 637-663, 2011.
- 651 Dean, R. G., & Dalrymple, R. A.: *Water wave mechanics for engineers and scientists* (Vol. 2, p. 353).
652 Singapore: World scientific., 1991.
- 653 Diaz, A. F.; Studzinski, C. D.; Mechoso C. R.: Relationships between precipitation anomalies in Uruguay
654 and Southern Brazil and sea surface temperature in the Pacific and Atlantic Oceans. *Journal of Climate*, 11,
655 251-271, 1998.
- 656 Dias, D. F.; Pezzi, L. P.; Gherardi, D. F. M.; Camargo, R.: Modeling the Spawning Strategies and Larval
657 Survival of the Brazilian Sardine (*Sardinella brasiliensis*). *Progress in Oceanography*, 123, 38–53, 2014.
- 658 Dean, R. G. & Dalryple, R. A.: *Water Wave Mechanics for Engineers and Scientists*. World Scientific, 2,
659 353, 1991.



- 660 Dudhia, J.: Numerical study of convection observed during the Winter Monsoon Experiment using a
661 mesoscale two-dimensional model. *Journal of Atmospheric Science*, 46, 3077–3107.
662 doi:10.1175/15200469(1989)046<3077:NSOCOD>2.0.CO;2PDF, 1989.
- 663 Egbert, G. D., & Erofeeva, S. Y.: The osu topex/poseidon global inverse solution tpxo. Oregon State
664 University, 2010.
- 665 Escobar, G. C.; Seluchi, M. E.; Andrade, K.: Synoptic classification of cold fronts associated with extremes
666 rainfall over the east of Santa Catarina state. *Brazilian Journal of Meteorology*, 31, 4, 649-661, 2016.
- 667 Evans, J. L. & Braun, A.: A climatology of subtropical cyclones in the South Atlantic. *Journal of Climate*,
668 25(21), 7328-7340, 2012.
- 669 Fandry, c. B.: Development of numerical model of tidal and wind-driven circulation in Bass Strait.
670 *Australian Journal of Marine Freshwater Research*, 32, 9-29, 1984.
- 671 Fewings, M. R.: Cross-shelf circulation and momentum and heat balances over the inner continental shelf
672 near Martha's Vineyard, Massachusetts doctoral dissertation, Massachusetts Institute of Technology and
673 Woods Hole Oceanographic Institution, 267, 2007.
- 674 Fetter, A. F. H. & Matano, R. P.: On the origins of the variability of the Malvinas Current in a global, eddy-
675 permitting, numerical simulation. *Journal of Geophysical Research*, 113, C11018,
676 Doi:10.1029/2008jc004875., 2008.
- 677 Figueiredo Jr., A. G.: Response of water column to strong wind forcing southern Brazilian inner shelf:
678 implications for sand ridge formation. *Marine Geology*, 35, 367-376, 1980.
- 679 Guimarães, P. V.; Farina, L.; Toldo Jr, E. E.; Analysis of extreme wave events on the southern coast of
680 Brazil. *Natural Hazards and Earth System Sciences*, 14(12), 3195-3205, 2014.
- 681 Gan, M.A. & Rao, V.B.: Surface cyclogenesis over South America. *Monthly Weather Review*, 119(5),
682 1293–1302, 1991.
- 683 Gill, A. E. & Clarke, A. J.: Wind-induced upwelling, coastal currents and sea-level changes. In *Deep Sea
684 Research and Oceanographic Abstracts*, Elsevier, 21, 5, 325-345, 1974.
- 685 Gozzo, L. F. & Da Rocha, R. P.: Air–sea interaction processes influencing the development of a Shapiro–
686 Keyser type cyclone over the subtropical South Atlantic Ocean. *Pure and Applied Geophysics*, 170(5),
687 917934, 2013.
- 688 Gozzo, L. F.; da Rocha, R. P.; Reboita, M. S.; Sugahara, S.: Subtropical cyclones over the southwestern
689 South Atlantic: Climatological aspects and case study. *Journal of Climate*, 27(22), 8543-8562, 2014.



- 690 Gramscianinov, C. B.; Hodges, K. I.; Camargo, R.: The properties and genesis environments of South
691 Atlantic cyclones. *Climate Dynamics*, 53(7-8), 4115-4140, 2019.
- 692 Gronholz, A.; Gräwe, U.; Paul, A.; Schulz, M.: Investigating the effects of a summer storm on the North
693 Sea stratification using a regional coupled ocean-atmosphere model. *Ocean Dynamics*, 67(2), 211-235,
694 2017.
- 695 Haidvogel, D. B.; Arango, H. G.; Hedstrom, K.; Beckmann, A.; Malanotte-Rizzoli, P.; Shchepetkin, A. F.:
696 Model evaluation experiments in the North Atlantic Basin: Simulations in nonlinear terrain-following
697 coordinates, *Dynamics of Atmosphere and Oceans*, 32, 239-281, 2000.
- 698 Hermes, J. C. & Reason, C. J. C.: Ocean model diagnosis of interannual coevolving SST variability in the
699 South Indian and South Atlantic Oceans. *Journal of Climate*, 18(15), 2864-2882, 2005.
- 700 Hong, S. Y.; Dudhia, J.; Chen, S. H.: A revised approach to ice microphysical processes for the bulk
701 parameterization of clouds and precipitation. *Monthly weather review*, 132(1), 103-120, 2004.
- 702 Hong, S. Y.; Noh, Y.; Dudhia, J.: A new vertical diffusion package with an explicit treatment of entrainment
703 processes, *Mon. Weather Rev.*, 134(9), 2318–2341, doi:10.1175/Mwr3199.1, 2006.
- 704 Hoskins, B. J. & Hodges, K. I.: A new perspective on southern hemisphere storm tracks. *Journal of Climate*,
705 18(20), 4108–4129, 2005.
- 706 Houghton, R. W. & Beer, T.: Wave propagation during the Ghana upwelling. *Journal of Geophysical*
707 *Research*, 81, 24, 4423-4429, 1976.
- 708 Innocentini, V. & Caetano Neto, E.: A case study of the 9 August 1998 south atlantic storm: Numerical
709 simulations of the wave activity. *Weather and Forecasting*, 11, 78–88, 1996.
- 710 Junker, T., Mohrholz, V., Schmidt, M., Siegfried, L., & van der Plas, A.: Coastal trapped wave propagation
711 along the southwest African shelf as revealed by moored observations. *Journal of Physical Oceanography*,
712 49(3), 851-866, 2019.
- 713 Kain, John S.: The Kain–Fritsch convective parameterization: An update. *Journal Appl. Meteor.*, 43, 170–
714 181. doi:10.1175/1520-0450(2004)043<0170:TKCPAU>2.0.CO ;2PDF, 2004.
- 715 Kantha, L. H. & Clayson, C. A.: *Numerical Models of Oceans and Oceanic Processes*. International
716 *Geophysics Series*, 66. Foreword by Kirk Bryan, Academic Press, 940, 2000.
- 717 Kitade, Y. & Matsuyama, M.: Coastal-trapped waves with several-day period caused by wind along the
718 southeast coast of Honshu, Japan. *Journal of oceanography*, 56(6), 727-744, 2000.



- 719 Kleczek, M. A.; Steeneveld, G. J.; Holtslag, A. A.: Evaluation of the weather research and forecasting
720 mesoscale model 4 for GABLS3: impact of boundary-layer schemes, boundary conditions and spin-up.
721 *Boundary-layer meteor.*, 152(2), 5 213-243, 2014.
- 722 Krüger, L. F.; da Rocha, R. P.; Reboita, M. S.; Ambrizzi, T.: RegCM3 nested in HadAM3 scenarios A2 and
723 B2: projected changes in extratropical cyclogenesis, temperature and precipitation over the South Atlantic
724 Ocean. *Climatic Change*, 113, 599-621, 2012.
- 725 Legeckis, R. & Gordon, A. L.: Satellite observations of the Brazil and Falkland Currents 1975 to 1976 and
726 1978. *Deep-Sea Research*, 29, 375-401, 1982.
- 727 Lentini, C. A. D.; Campos, E. J. D.; Podestá, G. P.: The annual cycle of satellite derived sea surface
728 temperature on the western South Atlantic shelf. *Brazilian journal of Oceanography*, 48 (2), 93–105, 2000.
- 729 Machado, A. A., Calliari, L. J., Melo Filho, E., & Klein, A. H. D. F. Historical assessment of extreme coastal
730 sea state conditions in southern Brazil and their relation to erosion episodes, *Pan-american Journal of*
731 *Aquatic Science*, 2011.
- 732 Machado, J. P.; Justino, F.; Souza, C. D.: Influence of El Niño-Southern Oscillation on baroclinic instability
733 and storm tracks in the Southern Hemisphere. *International Journal of Climatology*,
734 <https://doi.org/10.1002/joc.6651>, 2020.
- 735 Mascarenhas, A. S.; Miranda Jr., L. B.; Rock, N. J.: A study of oceanographic conditions in the region of
736 Cabo Frio, in *Fertility of the Sea*, 1, 285–308, Gordon and Breach, New York, 1971.
- 737 Matano, R. P.; Palma, E. D.; Piola, A. R.: The influence of the Brazil and Malvinas Currents on the
738 Southwestern Atlantic Shelf circulation. *Ocean Science*, 6, 983–995, 2010.
- 739 Matano, R. P.; V. Combes; A. R. Piola; R. Guerrero; E. D. Palma; P. T. Strub; C. James; H. Fenco; Y.
740 Chao; M. Saraceno.: The salinity signature of the cross-shelf exchanges in the southwestern Atlantic
741 Ocean: Numerical simulations, *J. Geophys. Res. Oceans*, 119, 7949-7968, doi:10.1002/2014JC010116,
742 2014.
- 743 Melo, E.; Romeu, M. A. R.; Hammes, G. R.: Reconstruction of sea state conditions at the Vitoria and Santa
744 Catarina coasts (Brazil during the June 2006 swell event. In. 7th International Conference on Coastal and
745 Port Engineering in Developing Countries, Dubai, 1-15, 2008.
- 746 Mendonça, L. F.; Souza, R. B.; Aseff, C. R. C.; Pezzi, L. P.; Möller, O. O.; Alves, R. C.: Regional modeling
747 of the water masses and circulation annual variability at the Southern Brazilian Continental Shelf, *Journal*
748 *of Geophysical Research, Oceans*, 121, DOI:10.1002/2016JC011780, 2017.



- 749 Mlawer, Eli. J.; Steven. J. T.; Patrick. D. B; Iacono, M. J.; Clough S. A.: Radiative transfer for
750 inhomogeneous atmospheres: RRTM, a validated correlated-k model for the longwave. *Journal of*
751 *Geophysical Res.*, 102, 16663–16682. doi:10.1029/97JD00237PDF, 1997.
- 752 Möller, O. O.; Piola, A. R.; Freitas, A. C.; Campos, E. J. D.: The effects of river discharge and seasonal
753 winds on the shelf off southeastern South America. *Continental Shelf Research*, 28, 1607-1624, 2008.
- 754 Niu, Guo–Yue, Zong–Liang Y., Kenneth E. M., Fei C., Michael B. E., Michael B., Anil K., Kevin M., Dev
755 N., Enrique R., M. T., Youlong X.: The community Noah land surface model with multiparameterization
756 options (Noah–MP): 1. Model description and evaluation with local–scale measurements. *Journal of*
757 *Geophysical Research*, 116, D12109. doi:10.1029/2010JD015139, 2011.
- 758 Olson, D. B.; Podestá, G. P.; Evans, R. H.; Brown, O.: Temporal variations in the separation of the Brazil
759 and Malvinas currents, *Deep-Sea Research*, 35, 1971-1990, 1988.
- 760 Palma, E. D.; Matano, R. P.; Piola, A. R.: A numerical study of the Southwestern Atlantic Shelf circulation:
761 Barotropic response to tidal and wind forcing. *Journal of Geophysical Research*, 109, C08014, 2004.
- 762 Palma, E. D.; Matano, R. P.; Piola, A. R.: A numerical study of the Southwestern Atlantic Shelf circulation:
763 Stratified ocean response to local and offshore forcing, *Journal of Geophysical Research*, 113, (C11),
764 C11010., 2008.
- 765 Palma, E. D. & Matano, R. P.: Disentangling the upwelling mechanisms of the South Brazil Bight,
766 *Continental Shelf Research*, 29, 1525– 1534, 2009.
- 767 Parise, C. K.; Calliari, L. J.; Krusche, N.: Extreme storm surges in the south of Brazil: atmospheric
768 conditions and shore erosion. *Brazilian Journal of Oceanography*, 57, 175-188, 2009.
- 769 Perlin, N.; Skillingstad, E. D.; Samelson, R. M.: Coastal atmospheric circulation around an idealized cape
770 during wind-driven upwelling studied from a coupled ocean–atmosphere model. *Monthly Weather Review*,
771 139(3), 809-829, 2011.
- 772 Pingree, R. D., & Mardell, G. T.: Slope turbulence, internal waves and phytoplankton growth at the Celtic
773 Sea shelf-break. *Philosophical Transactions of the Royal Society of London. Series A, Mathematical and*
774 *Physical Sciences*, 302(1472), 663-682, 1981.
- 775 Piola, A. R.; Campos, E. J. D.; Möller Jr, O. O.; Charo, M.; Martinez, C.: Subtropical Shelf Front off eastern
776 South America. *Journal of Geophysical Research*, 105, (C3), 6565–6578, 2000.
- 777 Piola, A. R.; Matano, R. P.; Palma, E. D.; Möller Jr, O. O.; Campos, E. J. D.: The influence of the Plata
778 River discharge on the western South Atlantic shelf. *Geophysical Research Letter*, 32, L01603, 2005.



- 779 Piola, A. R.; Möller Jr., O. O.; Guerrero, R. A.; Campos, E. J. D.: Variability of the Subtropical Shelf front
780 off eastern South America: winter 2003 and summer 2004. *Continental Shelf Research*, 28, 1639-1648,
781 2008.
- 782 Piola, A. R., Martínez Avellaneda, N., Guerrero, R. A., Jardon, F. P., Palma, E. D., & Romero, S. I.:
783 Malvinas-slope water intrusions on the northern Patagonia continental shelf. *Ocean Science*, 6(1), 345-359,
784 2010.
- 785 Ponte, R. M. & Gaspar, P.: Regional analysis of the inverted barometer effect over the global ocean using
786 TOPEX/POSEIDON data and model results. *Journal of Geophysical Research: Oceans*, 104(C7),
787 1558715601, 1999.
- 788 Powers, J. G., Klemp, J. B., Skamarock, W. C., Davis, C. A., Dudhia, J., Gill, D. O., Duda, M. G.: The
789 weather research and forecasting model: Overview, system efforts, and future directions. *Bulletin of the*
790 *American Meteorological Society*, 98(8), 1717-1737., 2017.
- 791 Pugh, D. T.: Tides, surges and mean sea level: A handbook for Engineers and Scientists. New York John
792 Wiley, 472, 1987.
- 793 Reale, M.; Liberato, M. L.; Lionello, P.; Pinto, J. G.; Salon, S.; Ulbrich, S.: A global climatology of
794 explosive cyclones using a multi-tracking approach. *Tellus A: Dynamic Meteorology and Oceanography*,
795 71(1), 1611340, 2019.
- 796 Reboita, M.S.; da Rocha, R.P.; Ambrizzi, T.; Sugahara, S.: South Atlantic Ocean cyclogenesis climatology
797 simulated by regional climate model RegCM3). *Climate Dynamics*, 35(7–8), 1331–1347, 2010.
- 798 Reboita, M. S.; Da Rocha, R. P.; Oliveira, D. M. D.: Key Features and adverse weather of the named
799 subtropical cyclones over the Southwestern South Atlantic Ocean. *Atmosphere*, 10(1), 6, 2019.
- 800 Reboita, M. S.; Reale, M.; da Rocha, R. P.; Giorgi, F.; Giuliani, G.; Coppola, E.; Cavazos, T.: Future
801 changes in the wintertime cyclonic activity over the CORDEX-CORE southern hemisphere domains in a
802 multi-model approach, 2020.
- 803 Reynolds, R. W.; Smith, T. M.; Liu, C.; Chelton, D. B.; Casey, K. S.; Schlax, M. G.: Daily High-
804 ResolutionBlended Analyses for Sea Surface Temperature. *Journal of Climate*, 20, 5473-5496, 2007.
- 805 Rocha, R. P.; Sugahara, S.; Silveira, R. B.: Sea waves generated by extratropical cyclones in the south
806 Atlantic Ocean: hindcast and validation against altimeter data. *Weather and Forecasting*, 19, 398–410, 2004.
- 807 Rocha, R. P.; Reboita, M. S.; Gozzo, L. F.; Dutra, L. M. M.; de Jesus, E. M.: Subtropical cyclones over the
808 oceanic basins: a review. *Annals of the New York Academy of Sciences*, 1436(1), 138-156, 2018.
- 809 Rodrigues, M. L. G.; Franco, D.; Sugahara, S.: Climatology of fronts in Santa Catarina coast. *Brazilian*
810 *Journal of Geophysics*, 22(2), 135-151, 2004.



- 811 Rosa, M. B.; Ferreira, N. J.; Gan, M. A.; Machado, L. H. R.: Energetics of cyclogenesis events over the
812 southern coast of Brazil. *Revista Brasileira de Meteorologia*, 28(3), 231-245, 2013.
- 813 Saldanha-Corrêa, F. M. P., & Gianesella, S. M. F.: A microcosm approach on the potential effects of the
814 vertical mixing of water masses over the primary productivity and phytoplankton biomass in the southern
815 Brazilian coastal region. *Brazilian Journal of Oceanography*, 52(3-4), 167-182, 2004.
- 816 Saraceno, M.; Provost, C.; Piola, A. R.: On the relationship between satellite-retrieved surface temperature
817 fronts and chlorophyll a in the western South Atlantic. *Journal of Geophysical Research: Oceans*, 110(C11),
818 2005.
- 819 Schossler, V.; Aquino, F. E.; Reis, P. A.; Simões, J. C.: Antarctic atmospheric circulation anomalies and
820 explosive cyclogenesis in the spring of 2016. *Theoretical and applied climatology*, 2020.
- 821 Shchepetkin, A. F. & J. C. McWilliams: The Regional Ocean Modeling System: a split explicit, freesurface,
822 topography-following coordinates ocean model. *Ocean Modelling*, 9, 347–404, 2005.
- 823 Shchepetkin, A. F. & McWilliams, J. C.: Correction and Commentary for "Ocean Forecasting in
824 TerrainFollowing Coordinates: Formulation and Skill Assessment of the Regional Ocean Modeling System"
825 by Haidvogel *et al.*, *Journal of Computational Physics*. 227, 3595-3624. *Journal of Computational Physics*,
826 228, 8985-9000, 2009.
- 827 Schumann, E. H.: Long-period coastal trapped waves off the southeast coast of Southern Africa. *Continental
828 Shelf Research*, 2, 2-3, 97-107, 1983.
- 829 Skamarock, W. C.; Klemp J. B.; Dudhia J.; Gill, D. O.; Barker, D. M., Duda M.G.; Huang, X. Y.; Wang,
830 W.; Powers, J. G.: A description of the Advanced Research WRF version 3. NCAR Tech. Note
831 NCAR/TN475+STR, 113, 2008.
- 832 Souza, R. B. & Robinson, I. S.: Lagrangian and satellite observations of the Brazilian Coastal Current.
833 *Continental Shelf Research*, 24, 241-262, 2004.
- 834 Souza, R. B. Mata, M. M.; Garcia, C. A. E.; Kampel, M.; Oliveira, E. N.; Lorenzetti, J. A.: Multi-sensor
835 satellite and in situ measurements of a warm core ocean eddy south of the Brazil-Malvinas Confluence
836 region. *Remote Sensing Environmental*, 100, 52-66, 2006.
- 837 Stech, J. L. & Lorenzetti, J. A.: The response of the South Brazil bight to the passage of wintertime cold
838 fronts. *Journal of Geophysical Research*, 97, C6, 9507–9520, 1992.
- 839 Strub, P. T.; James, C.; Combes, V.; Matano, R. P.; Piola, A. R.; Palma, E. D.; Saraceno, M.; Guerrero, R.
840 A.; Fenco, H.; Ruiz-Etcheverry, L. A.: Altimeter-derived seasonal circulation on the southwest Atlantic
841 shelf: 27, 8-43, 8°S. *Journal of Geophysical Research - Oceans*, 120, 2015.



- 842 Sun, X., Cook, K. H., & Vizy, E. K.: The South Atlantic subtropical high: climatology and interannual
843 variability. *Journal of Climate*, 30(9), 3279-3296, 2017.
- 844 Taguchi, B.; Nakamura, H.; Nonaka, M.; Komori, N.; Kuwano-Yoshida, A.; Takaya, K.; Goto, A.: Seasonal
845 evolutions of atmospheric response to decadal SST anomalies in the North Pacific subarctic frontal zone:
846 Observations and a coupled model simulation. *Journal of Climate*, 25(1), 111-139, 2012.
- 847 Tang, Y. M. & Grimshaw, R.: A modal analysis of coastally trapped waves generated by tropical cyclones.
848 *Journal of Physical Oceanography*, 25(7), 1577-1598, 1995.
- 849 Thompson, K. R.: The response of Southern North Sea elevation to oceanographical and meteorological
850 forcing. *Estuarine, Coastal and Shelf Science*, 13, 287-301, 1981.
- 851 Thompson, R.: Low-pass filters to suppress inertial and tidal frequencies. *Journal of Physical Oceanography*,
852 13, 6, 1077–1083, 1983.
- 853 Truccolo, E. C.; Franco, D.; Schettini, C. A. F.: The low frequency sea level oscillations in the northern
854 coast of Santa Catarina, Brazil. *Journal of Coastal Research*, 547-552, 2004.
- 855 Yao, T.; Freeland, H. J.; Mysak, L. A.: A comparison of low-frequency current observations off British
856 Columbia with coastal-trapped wave theory. *Journal of physical oceanography*, 14(1), 22-34, 1984.
- 857 Wallace, J. M. & Hobbs P. V.: *Atmospheric Science: An Introductory Survey*. Academic Press, Inc, London,
858 467, 1977.
- 859 Warner, J. C.; Sherwood, C. R.; Signell, R. P.; Harris, C.; Arango H. G.: Development of a threedimensional,
860 regional, coupled wave, current, and sediment-transport model. *Computers and Geosciences*, 34, 1284–
861 1306, 2008.
- 862 Wienders, N.; Arhan, M.; Mercier, H.: Circulation at the western boundary of the South and Equatorial
863 Atlantic: Exchanges with the ocean interior. *Journal of Marine Research*, 58, 1007-1039, 2000.
- 864 Wunsch, C. & Stammer, D.: Atmospheric Loading and the Oceanic “Inverted Barometer” Effect. *Reviews*
865 *of Geophysics*, 35 (1), 79-107, 1997.
- 866 Zavialov, P.; Möller, O. O. Jr.; Campos, E.: First direct measurements of currents on the continental shelf
867 of Southern Brazil. *Continental Shelf Research*, 22: 1975-1986, 2002.
- 868 Zenbruski, S.; Barreto, T. H.; Palma, J. C.; Milliman, J. D. Preliminary study of geomorphological
869 provinces of the Brazilian continental margin. *Brazilian Congress of Geology*, 2, 187-209, 1972.